Delft University of Technology

Document Version
Final published version

Licence
CC BY-NC-ND

Citation (APA)
Chen, J., Li, Z., Yang, B., Hu, X., Li, W., Li, Z., Yan, X., Zhang, G., Fan, J., & More Authors (2026). Long-term high-temperature aging mechanism of copper-metallized through-glass vias: a combined nanoindentation test and hybrid Potts-phase field simulation study. *Microsystems and Nanoengineering*, *12*(1), Article 46. https://doi.org/10.1038/s41378-026-01160-0

Important note
To cite this publication, please use the final published version (if applicable).
Please check the document version above.

Copyright
In case the licence states “Dutch Copyright Act (Article 25fa)”, this publication was made available Green Open Access via the TU Delft Institutional Repository pursuant to Dutch Copyright Act (Article 25fa, the Taverne amendment). This provision does not affect copyright ownership.
Unless copyright is transferred by contract or statute, it remains with the copyright holder.

Sharing and reuse
Other than for strictly personal use, it is not permitted to download, forward or distribute the text or part of it, without the consent of the author(s) and/or copyright holder(s), unless the work is under an open content license such as Creative Commons.

Takedown policy
Please contact us and provide details if you believe this document breaches copyrights.
We will remove access to the work immediately and investigate your claim.

This work is downloaded from Delft University of Technology.

Chen et al. *Microsystems & Nanoengineering* (2026)12:46
https://doi.org/10.1038/s41378-026-01160-0

Microsystems & Nanoengineering
www.nature.com/micronano

ARTICLE Open Access

Long-term high-temperature aging mechanism of copper-metallized through-glass vias: a combined nanoindentation test and hybrid Potts-phase field simulation study

Junwei Chen[1], Zezhan Li[1], Bin Yang[2,4], Xiao Hu[3]✉, Wenyu Li[1], Zichuan Li[3], Xuyang Yan[1], Zhoudong Yang[1], Jiao Liang[1], Guannan Yang[2,4], Chao Gu[1], Changran Zheng[1], Chengqiang Cui[2,4]✉, Guoqi Zhang[3] and Jiajie Fan[1,3,5]✉

Abstract

The reliability of through-glass via (TGV) interconnects is critical for advanced semiconductor packaging. This work investigates microstructural and mechanical evolution in electroplated TGV–Cu subjected to long-term aging at 250 °C. TGV samples were fabricated via laser-induced etching and double-sided copper electroplating, then aged for up to 1008 h. Nanoindentation revealed region-dependent reductions in hardness (from 2.0–2.5 GPa to below 0.5 GPa) and modulus (from 110–130 GPa to 40–90 GPa), with surface-near regions most affected. The glass substrate maintained stable mechanical properties until microcracks formed after 1008 h. EBSD quantification showed grain-size enlargement from 0.46 μm to 1.86 μm and a concurrent decrease in dislocation density. Molecular dynamics simulations of 3, 4, 5 nm grains corroborated the inverse relationship between grain size and micro-mechanical properties. A hybrid Potts-phase field model further linked grain coarsening to stress relaxation and elastic-energy minimization, revealing that as grains grow, the overall von Mises stress in the structure decreases; high-modulus grains retain relatively higher local stresses, while low-modulus, low-stress grains exhibit faster growth rates. Electrical I–V measurements confirmed stable ohmic behavior, despite a drop in insulation resistance. These integrated experimental and computational insights provide theoretical guidance for optimizing TGV interposer design and ensuring long-term operational reliability in heterogeneous integration technologies.

Introduction

The computing demands of future data-intensive applications will greatly exceed the capabilities of current electronics, and are unlikely to be met by isolated improvements in transistors, data storage technologies, or integrated circuit architectures alone[1]. Consequently, advanced packaging techniques leveraging system miniaturization and heterogeneous integration have emerged as critical solutions to overcome performance bottlenecks[2]. Among these approaches, 2.5D packaging integrates multiple chips in-plane through silicon or glass interposers, facilitating more compact, lightweight, and functionally integrated systems, thus markedly improving spatial efficiency[3,4]. Through-via technology, embedded within interposers, vertically connects dies to underlying electrodes, significantly enhancing inter-chip signal transmission density, speed, and efficiency, and has been widely adopted in heterogeneous integration[5]. Nevertheless, conventional through-silicon via (TSV) technology suffers from inherent limitations, including complex fabrication processes, high costs, and significant electromagnetic coupling due to silicon's semiconducting properties, restricting its suitability for high-frequency and large-scale applications[6,7]. In contrast, through-glass via

Correspondence: Xiao Hu (x.hu-1@tudelft.nl) or
Chengqiang Cui (cqcui@gdut.edu.cn) or Jiajie Fan (jiajie_fan@fudan.edu.cn)
[1]Shanghai Engineering Technology Research Center of SiC Power Device, College of Intelligent Robotics and Advanced Manufacturing, Fudan University, Shanghai, China
[2]State Key Laboratory of Precision Electronic Manufacturing Technology and Equipment, Guangdong University of Technology, Guangzhou, China
Full list of author information is available at the end of the article

© The Author(s) 2026
Open Access This article is licensed under a Creative Commons Attribution-NonCommercial-NoDerivatives 4.0 International License, which permits any non-commercial use, sharing, distribution and reproduction in any medium or format, as long as you give appropriate credit to the original author(s) and the source, provide a link to the Creative Commons licence, and indicate if you modified the licensed material. You do not have permission under this licence to share adapted material derived from this article or parts of it. The images or other third party material in this article are included in the article's Creative Commons licence, unless indicated otherwise in a credit line to the material. If material is not included in the article's Creative Commons licence and your intended use is not permitted by statutory regulation or exceeds the permitted use, you will need to obtain permission directly from the copyright holder. To view a copy of this licence, visit http://creativecommons.org/licenses/by-nc-nd/4.0/.

(TGV) technology, utilizing glass substrates, exhibits notable advantages such as reduced costs, superior thermal stability, and excellent high-frequency electrical performance, making it increasingly attractive for diverse applications in RF components, optoelectronic integration, micro-electromechanical systems (MEMS), and other emerging technologies[8,9].

To further enhance interconnect density and ensure long-term operational reliability, there is increasing industry interest in through-glass via (TGV) structures that integrate the benefits of copper filling via electroplating with conformal metallization techniques[8,10–12]. A TGV interposer has been successfully fabricated utilizing laser-induced deep etching followed by via-filling processes[13]. However, as via diameters continue to shrink and aspect ratios (defined as via depth to diameter) increase, significant anisotropic internal stresses develop within the vias. These stresses can lead to reliability concerns, including copper extrusion, interface delamination, and substrate cracking[14–16]. Post-electroplating, copper grains within vias exhibit random orientations without a defined structural order[17–19]. During short-term post-plating annealing, copper in TGV typically undergo recovery, recrystallization, and grain growth phases, during which grain size, morphology, and defect density evolve dynamically[17,20,21]. Consequently, the strain distribution within the Cu filling of the TGVs becomes highly heterogeneous, with varying degrees of plastic deformation across different grain regions, dependent on their spatial positions[22–24]. Concurrently, residual stresses evolve in response to these microstructural transformations[25]. Quantitative links between heterogeneous microstructures and key mechanical properties are still scarce[26]. Experimentally tracking the coupled evolution of these microstructures under thermomechanical loading and during long term aging is technically demanding and time-consuming. Integrating high-resolution computational approaches with advanced characterization methods offers a promising solution. Molecular dynamics (MD) simulations capture the nanoindentation process at atomic resolution and directly correlate grain-scale features with micro-mechanical responses[27,28]. Phase field modeling can combine Monte Carlo with multiphysics coupling to simulate microstructural evolution across time scales beyond experimental reach[22,29]. Together, these multiscale techniques establish a framework for assessing the long-term reliability of TGV-Cu interconnects.

In this paper, we combine experiment and multiscale simulations to unravel how long-term aging at 250 °C alters TGV–Cu interconnects. Spatially resolved nanoindentation and EBSD characterize the relationship between micro-mechanical properties and grain-growth kinetics. Molecular dynamics simulations then explore the theoretical dependence of hardness and elastic modulus on grain size. A hybrid Q-state Potts-phase field model links grain-morphology evolution with stress relaxation and free-energy minimization, examining the interplay between grain structure and thermo-mechanical behavior. Finally, I–V measurements confirm the stability of the electrical performance under prolonged aging.

Results and Discussion

Figure 1a illustrates the fabrication process for the TGV-Cu interposer. In this study, a conventional Schott AF32 borosilicate glass substrate was used. Through a laser-induced etching process, through-glass vias with a diameter of 50 μm and a thickness of 300 μm were formed, and via metallization was achieved by double-sided copper electroplating. Initially, a high-current-density DC flash plating rapidly deposits a dense initial layer on via walls. The process then shifts to AC plating to ensure uniform growth in the via center, completing bridging. Finally, low-current-density DC plating thickens the copper layer to the required design specifications and thickness. The finished TGV-Cu samples were aged at 250 °C for durations of 0, 84, 168, 504, and 1008 hours. Samples were then sectioned, mounted, and polished to expose cross-sections for further study.

As structural dimensions decrease below a certain size, the mechanical properties of materials, influenced significantly by surface effects, microstructure, and processing history, often differ notably from bulk materials[30]. Nanoindentation is widely used to measure mechanical properties at the micro and nanoscale due to its high sensitivity and resolution[31]. In this study, elastic modulus (E) and hardness (H) were measured using a Nano-indenter XP system (MTS Systems Corporation) with a dynamic contact module (DCM) and continuous stiffness measurement (CSM) at a constant strain rate of $0.05\ s^{-1}$. A standard Berkovich diamond tip was used, continuously recording penetration depth (h) and applied load (P) during indentation. Load-displacement curves were used to calculate E and H based on the contact area. The specific indentation locations are shown in Fig. 1b. Figure S1 presents the load-displacement curves for TGV-Cu under a fixed 50 mN load after different aging periods. The maximum indentation depth remained below 10% of the copper thickness, avoiding any substrate effects from the glass. These curves show that both the maximum and residual indentation depths change with aging time, indicating corresponding variations in hardness and modulus of the copper layer.

The Oliver-Pharr method was used to calculate hardness (H) and elastic modulus (E) according to the

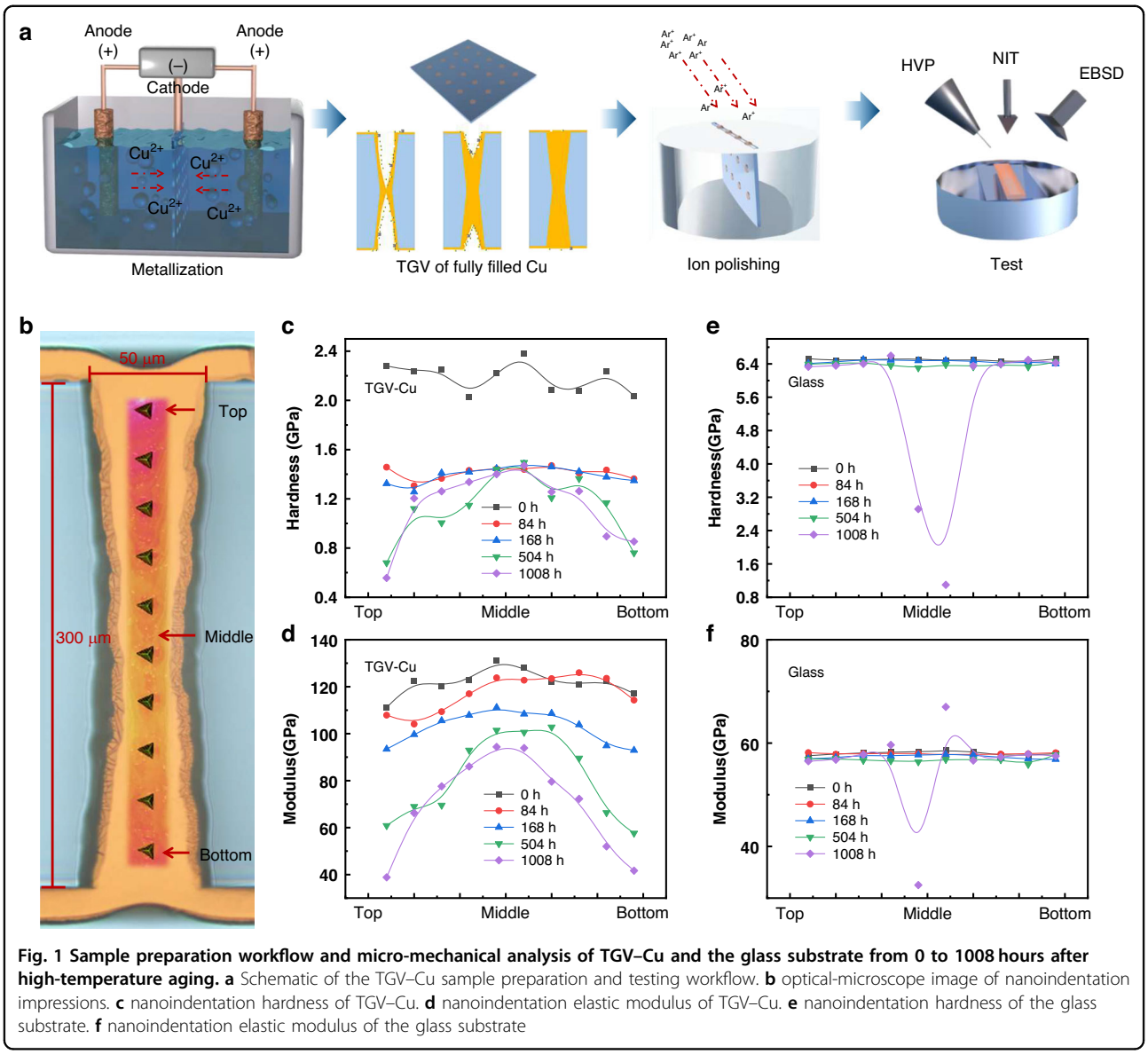


Fig. 1 Sample preparation workflow and micro-mechanical analysis of TGV–Cu and the glass substrate from 0 to 1008 hours after high-temperature aging. a Schematic of the TGV–Cu sample preparation and testing workflow. **b** optical-microscope image of nanoindentation impressions. **c** nanoindentation hardness of TGV–Cu. **d** nanoindentation elastic modulus of TGV–Cu. **e** nanoindentation hardness of the glass substrate. **f** nanoindentation elastic modulus of the glass substrate

following equations[14,32]:

$$H = \frac{P_{\max}}{A} \tag{1}$$

$$\frac{1}{E_r} = \frac{1-\nu^2}{E} + \frac{1-\nu_i^2}{E_i} \tag{2}$$

In the above formula, $P_{\max}$ is the maximum load, and A is the contact area of the indentation. For the Berkovich indenter, the constant β is 1.034, E_r is the effective elastic modulus, and E_i and υ_i are the elastic modulus (1140 GPa) and Poisson's ratio (0.07) of the indenter, respectively.

Figure 1c, d show changes in hardness and elastic modulus of TGV-Cu over the aging period. Initially, the hardness was between 2.0 and 2.5 GPa, rapidly declining to around 1.5 GPa after 84 hours, and gradually decreasing afterward. The Mid-region hardness showed only slight changes after 84 hours, whereas the Top and Bottom regions continuously declined to below 0.5 GPa. Similarly, the elastic modulus dropped from 110–130 GPa initially to 40–90 GPa after 1008 hours, with the Mid-region declining more slowly than the Top and Bottom regions. These results indicate that prolonged high-temperature aging progressively reduces hardness and modulus, with the regions near via surfaces most affected.

Figure 1e, f present nanoindentation results for the glass substrate approximately 10–20 μm from the TGV-Cu/glass interface. The glass hardness remained stable at approximately 6.3–6.5 GPa and the modulus around 56–58 GPa from 0 to 504 hours. However, after 1008 hours, a sharp decline in hardness and abnormal modulus behavior were observed in the Mid-region. Optical microscopy (Fig. S2) and SEM imaging (Fig. S3) show microcracks in the glass after prolonged aging and reveal that the outliers correspond to indentations intersecting these cracks rather than intrinsic degradation of the glass. To verify this, we performed additional nanoindentation in crack-free (located >50 μm away from any visible surface or subsurface cracks) under the same CSM conditions. After applying an exclusion criterion to remove crack-affected indents, the representative glass properties at 1008 h remain essentially unchanged relative to earlier times ($H = 6.4 \pm 0.2$ GPa; $E = 57.1 \pm 0.7$ GPa). Measurements at the same positional region for other aging times likewise show similarly stable properties; load-displacement curves are shown in Fig. S1c. These results confirm that the previous anomaly arose from indents intersecting microcracks, whereas the intrinsic, crack-free glass remains mechanically stable up to 1008 h.

The high dislocation and grain-boundary densities in TGV-Cu, along with its complex grain orientations and sizes, make its mechanical properties sensitive to microstructural evolution. A systematic EBSD analysis of TGV-Cu microstructures before and after aging was conducted in a region measuring 10 μm (width) × 300 μm (length), matching the nanoindentation area.

Figure 2a shows inverse pole figure (IPF) maps for samples aged for 0 and 1008 hours, and Fig. 2b provides corresponding grain-size distributions. During aging at 250 °C, grain size increased rapidly from an average diameter of 0.46 μm (0 hours) to 1.26 μm after 84 hours—a nearly 300 % increase—aligning with the significant decrease in hardness and modulus observed. Further aging slowed grain growth, reaching an average diameter of 1.86 μm by 1008 hours, representing a roughly 30% increase compared to the 84-hour measurement.

Table 1 summarizes grain-size changes in the Top, Middle, and Bottom regions of the via (each 10 μm × 15 μm). Initially (0 hours), grain sizes were similar across all regions. However, after aging, grains near the via openings (Top and Bottom) grew significantly from 1.44 μm at 84 hours to 1.99 μm at 1008 hours. Conversely, grains in the Middle region grew more slowly, increasing from 1.20 μm to 1.34 μm over the same aging period. This regional disparity explains the slower hardness reduction in the Middle region and the pronounced microcracking observed in the underlying glass substrate after 1008 hours.

During prolonged aging at 250 °C, electroplated copper first undergoes recovery and recrystallization, releasing stored energy within grains. Electroplated copper typically has a fine-grained structure with high dislocation density, causing recrystallization at temperatures well below copper's melting point, making 250 °C sufficient for this process. Recrystallization produces randomly oriented equiaxed grains and significantly reduces dislocation density[33].

Figure 2c, d present the statistical distribution and spatial maps of geometrically necessary dislocation (GND) density in selected EBSD scan regions. As grain size increases, dislocation density decreases, dropping rapidly from an initial $1.98 \times 10^{16}\ m^{-2}$ (0 hours) to $9.32 \times 10^{15}\ m^{-2}$ after 84 hours, and gradually to $3.82 \times 10^{15}\ m^{-2}$ by 1008 hours. This indicates that high-temperature aging significantly reduces internal dislocation density in electroplated copper. Overall, aging at 250 °C significantly accelerates copper grain growth, homogenizes grain orientations, reduces both dislocation density and grain-boundary area, and thereby lowers the material's lattice distortion energy, stabilizing a low-dislocation microstructure.

To clarify how copper grain size affects mechanical properties, MD simulations were conducted on polycrystalline copper models with average grain sizes of 3, 4 and 5 nm[34]. A rigid Berkovich diamond indenter probed a simulation cell measuring 200 × 200 × 260 Å containing approximately 691,483 atoms; grain sizes were controlled by varying the number of grains within the fixed cell. During loading and unloading, the indenter advanced at 2.6 Å/ps to a maximum penetration depth of 4 nm. The system was then equilibrated for 30 ps at 25 °C in an NPT ensemble with a Nose–Hoover thermostat and a 1 fs time step, using periodic boundary conditions and initial energy minimization via the conjugate gradient method. Figure 3a–c presents the atomic configurations and indentation morphologies for each model, while Fig. 3d shows the corresponding load–displacement curves. The 3 nm sample exhibited the highest peak load, and serrations during loading–unloading indicate dislocation-mediated plasticity and work hardening. Hardness and elastic modulus were calculated by the Oliver–Pharr method ($\varepsilon = 0.75$; $A = 24.5\ hc^2$). As shown in Fig. 3e, hardness decreases from 0.50 GPa at 3 nm to 0.43 GPa at 5 nm; modulus follows a similar trend, falling from 24 GPa to 19.3 GPa. These simulations corroborate experimental findings that larger copper grains reduce micromechanical strength in TGV–Cu[35,36]. The MD cell deliberately employs periodic boundary conditions and 3–5 nm grains to isolate grain-boundary-mediated indentation mechanisms (partial dislocation activity at grain boundaries with limited grain boundary sliding). This configuration is therefore used qualitatively to confirm the monotonic grain-size trend ($\partial(H, E)/\partial d < 0$) rather than to extrapolate absolute magnitudes to the sub-micron

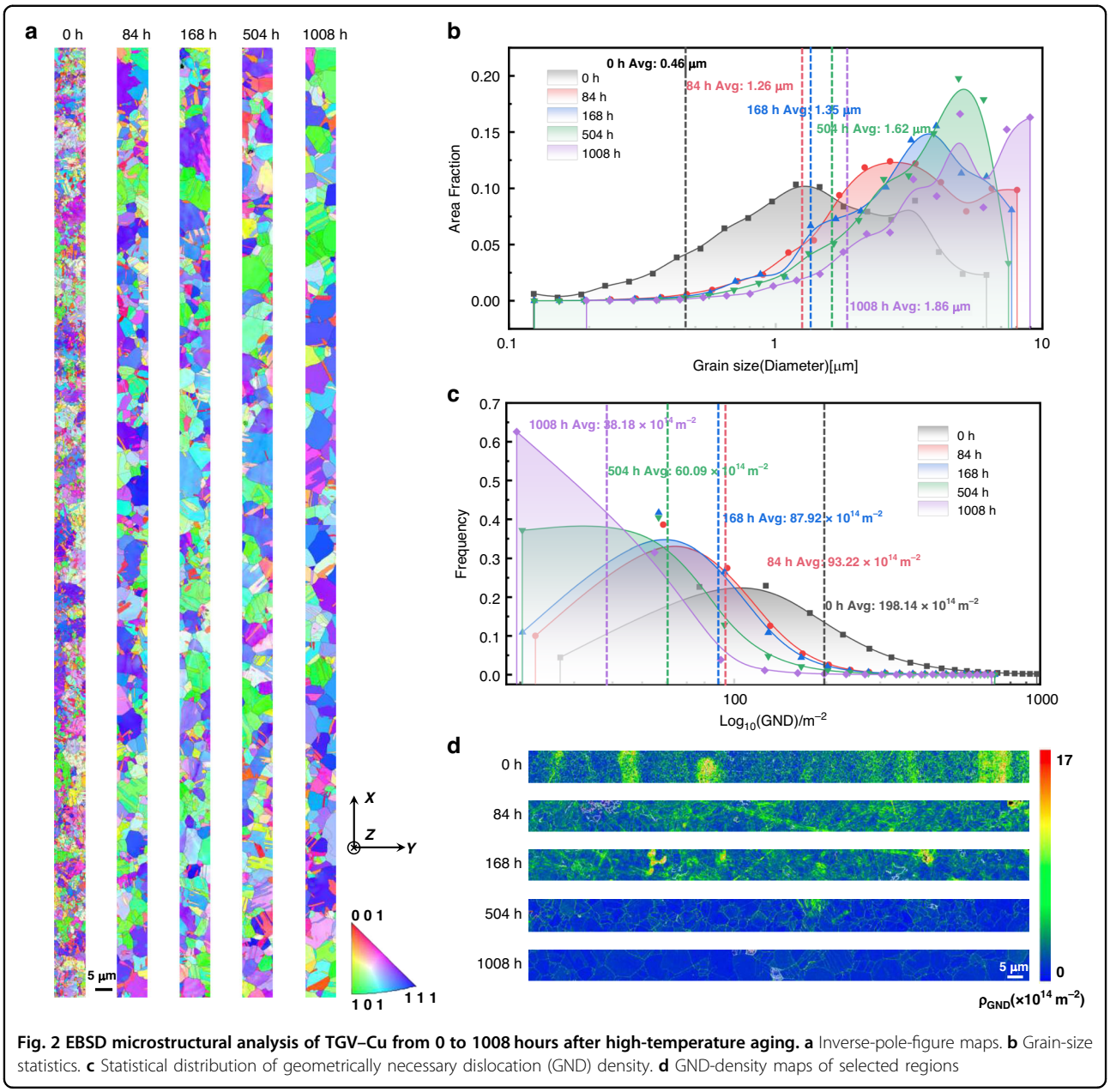


Fig. 2 EBSD microstructural analysis of TGV–Cu from 0 to 1008 hours after high-temperature aging. a Inverse-pole-figure maps. **b** Grain-size statistics. **c** Statistical distribution of geometrically necessary dislocation (GND) density. **d** GND-density maps of selected regions

Table 1 Grain-size statistics for the Top, Middle, and Bottom regions of the TGV

Average grain size(μm)	0	84 h	168 h	504 h	1008 h
Top	0.56	1.44	1.54	1.78	1.99
Middle	0.58	1.20	1.23	1.28	1.34
Bottom	0.52	1.18	1.31	1.50	1.97

experimental regime, where plasticity is dislocation-controlled and follows conventional Hall–Petch behavior.

Thermo-mechanical responses in TGV–Cu depend critically on copper grain morphology, orientation, and spatial distribution[37]. Experimentally, EBSD measurements show that the average Cu grain diameter within TGV increased from approximately 0.46 μm to 1.86 μm as aging progressed from 0 to 1008 hours at 250 °C. To investigate the microstructural evolution and thermomechanical behavior of Cu grains in TGV at an aging temperature of 250 °C, a hybrid Q-state Pottsphase field model was developed. This model integrates Monte Carlo methods for discrete grain evolution with the Allen-Cahn phase-field approach for continuous order parameter dynamics, coupled with thermomechanical calculations to account for thermal, elastic, and plastic strains[38,39].

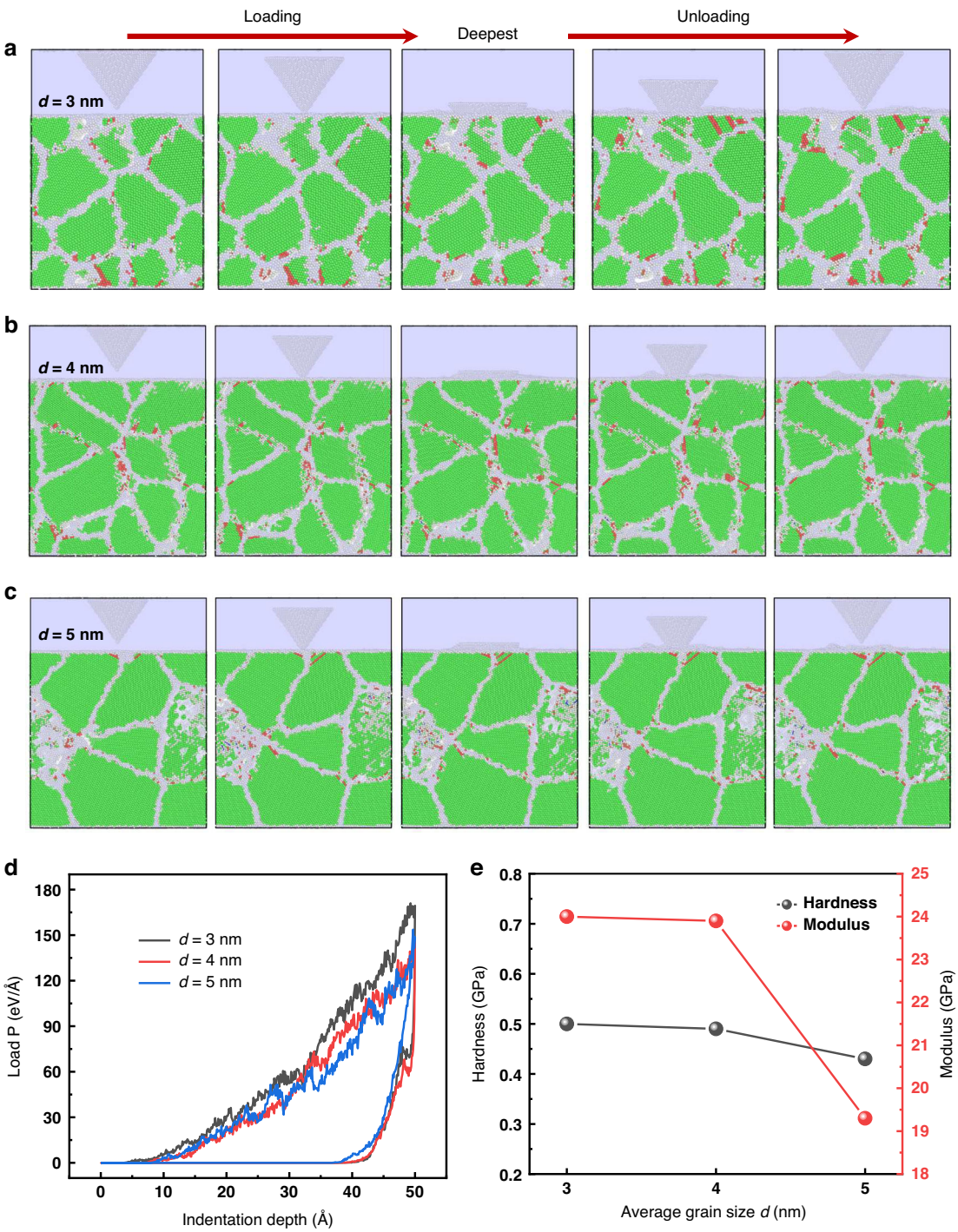


Fig. 3 Molecular dynamics simulation results for nanoindentation of polycrystalline copper: loading–unloading curve. a the 3 nm grain-size model; **b** the 4 nm grain-size model; **c** the 5 nm grain-size model. **d** force versus indentation depth for different grain sizes. **e** simulated hardness and elastic modulus as a function of grain size

In the class Potts model, the microstructure is discretized into a regular lattice grid, and each lattice site is assigned a discrete state $q \in 0, 1, \ldots, Q-1$, representing distinct Cu grain orientations. The total energy of the system is defined as:

$$E_{Potts} = \sum_{i,j} J_{q_i,q_j}(1 - \delta_{q_i,q_j}) \quad (3)$$

Where J_{q_i,q_j} represents the interaction energy between neighboring grain states, and δ_{q_i,q_j} is the Kronecker delta, equaling 1 when $q_i = q_j$ (indicating sites within the same grain) and 0 otherwise (indicating sites on a grain boundary). The evolution of the system is governed by the Metropolis algorithm. The energy difference ΔE resulting from this proposed change is calculated, and the acceptance of the new state is determined using the probability:

$$P_{accept}(\Delta E) = \frac{1}{1 + e^{\Delta E/(k_B T)}} \tag{4}$$

The hybrid Potts–Phase field model introduces continuous order parameters $\eta_q(i,j)$ for each site(i,j) and q denoting the grain orientations, $\eta_q = 1$ indicates the site (i,j) belongs to a grain with orientation q. The order parameters evolve according to the Allen-Cahn equation:

$$\frac{\partial \eta_q}{\partial t} = -L\frac{\partial F}{\partial \eta_q} \tag{5}$$

where $L = 4m/3l_{GB}$ is the mobility, m is the temperature-dependent grain boundary mobility calculated by $m = m_0 \exp(-Q_{act}/k_B T)$, in which m_0 is the pre-exponential factor, and Q_{act} is the activation energy. The total free energy functional F is defined as:

$$F = \sum_{i,j}\left(\sum_{q=0}^{Q-1}\left[k\eta_q^2(1-\eta_q)^2 + \alpha\sum_{q_i \neq q_j}\eta_{q_i}^2\eta_{q_j}^2\right] + \kappa_\eta\sum_{q=0}^{Q-1}(\nabla\eta_q)^2 + E_{el}\right) \tag{6}$$

where k and α are the bulk energy coefficients, κ_η is the gradient energy coefficient, and E_{el} represents the elastic energy contribution. In the hybrid model, the energy change ΔE_{hybrid} is calculated as:

$$\Delta E_{hybrid} = \Delta E_{Potts} + \Delta E_{bulk} + \Delta E_{grad} + \Delta E_{elastic} \tag{7}$$

A strain energy term E_{el} is introduced to capture the impact of thermo-elasto-plastic effects on the microstructure evolution. Assuming an additive decomposition of elastic, thermal, and plastic contributions to total strain, Cauchy strain can be written in the following expression:

$$\varepsilon = \varepsilon_{\mathrm{el}} + \varepsilon_{\mathrm{th}} + \varepsilon_{pl} \tag{8}$$

Thermal strain was calculated as:

$$\varepsilon_{\mathrm{th}} = \alpha_{\mathrm{th}}\Delta T \tag{9}$$

where α_{th} is the coefficient of thermal expansion (CTE) for Cu ($\alpha_{\mathrm{th}} = 17\times10^{-6},^{\circ}\mathrm{C}^{-1}$), and ($\Delta T = 250^{\circ}\mathrm{C} - 25^{\circ}\mathrm{C} = 225^{\circ}\mathrm{C}$) is the temperature difference from the reference state. For the Cu/Glass interface, the glass CTE ($\alpha_{\mathrm{th,Glass}} = 3.2\times10^{-6},^{\circ}\mathrm{C}^{-1}$) was applied to interface points, introducing a thermal strain mismatch that induces additional interfacial stress.

Elastic strain is derived from the global strain field, adjusted by subtracting thermal and plastic strains:

$$\varepsilon_{\mathrm{el}} = \varepsilon - \varepsilon_{\mathrm{th}} - \varepsilon_{pl} \tag{10}$$

A plane strain assumption was made to simplify the thermo-elasto-plastic calculation. Considering the periodic cell extended infinitely, the global strain field is computed using a fast Fourier transform (FFT)-based approach. Elastic properties were defined using anisotropic elastic constants ($E_1, E_2, E_3, \nu_{12}, \nu_{13}, \nu_{23}$) for 12 Cu orientations, as Table S1. For glass interface regions, a Young's modulus of 74.8 GPa and Poisson's ratio of 0.24 were used. The stiffness matrix for each site (i,j) was defined as:

$$C = \begin{bmatrix} C_{11} & C_{12} & 0 \\ C_{12} & C_{11} & 0 \\ 0 & 0 & C_{44} \end{bmatrix}, \tag{11}$$

where,

$$C_{11} = \frac{E_{avg}}{1-\nu_{avg}^2}, C_{12} = \frac{\nu_{avg}E_{avg}}{1-\nu_{avg}^2}, C_{44} = \frac{E_{avg}}{2(1+\nu_{avg})}. \tag{12}$$

where E_{avg} and ν_{avg} are averaged elastic constants adjusted for different Cu orientations and Cu/Glass interfaces.

According to Stress-strain relationship:

$$\sigma = \begin{bmatrix} \sigma_{xx} \\ \sigma_{yy} \\ \sigma_{xy} \end{bmatrix} = C \cdot \begin{bmatrix} \varepsilon_{xx} \\ \varepsilon_{yy} \\ \varepsilon_{xy} \end{bmatrix} \tag{13}$$

the stress tensors' components were calculated as:

$$\begin{aligned} \sigma_{xx} &= C_{11}\varepsilon_{xx}^{el} + C_{12}\varepsilon_{yy}^{el}, \\ \sigma_{yy} &= C_{12}\varepsilon_{xx}^{el} + C_{11}\varepsilon_{yy}^{el}, \\ \sigma_{xy} &= C_{44}\varepsilon_{xy}^{el}. \end{aligned} \tag{14}$$

The elastic energy was computed as:

$$E_{el} = \frac{1}{2}\varepsilon_{el} : \sigma \tag{15}$$

where ε_{el} and σ are the elastic strain and stress tensors, respectively. The von Mises equivalent stress is computed to assess plastic flow

$$\sigma_{vm} = \sqrt{\sigma_{xx}^2 - \sigma_{xx}\sigma_{yy} + \sigma_{yy}^2 + 3\sigma_{xy}^2} \tag{16}$$

Plastic deformation was modeled using the von Mises yield criterion, with yield strength dependent on grain size via the Hall-Petch relationship:

$$\sigma_Y = \sigma_0 + \frac{k_Y}{\sqrt{d}} \tag{17}$$

where $\sigma_0 = 20\,\mathrm{MPa}$, $k_Y = 0.14\,\mathrm{MPa}\cdot\mathrm{m}^{1/2}$, and d is the grain diameter.

The hybrid model is simulated with a specified number of Monte Carlo steps, and the following operations are performed in each MC step; the input parameters are presented in Table S2: First, the lattice map evolution is performed based on the Potts model with Glauber dynamics. Then, order parameters are evolved according to the Allen-Cahn equation with thermal-mechanical coupling based on the finite difference method. The global strain field with periodic boundary conditions is calculated by fast Fourier transform (FFT) to update the elastic energy, calculate von Mises stress, and the plastic strain field. The grain size is counted, and the yield strength is calculated as the next plastic deformation criterion.

The simulation results are shown in Fig. 4. During aging from 0 to 1008 h, copper grains in the TGV rapidly coarsen from a fine, random distribution, with a growth rate that is initially fast and then slows (Fig. 4a). To ensure consistency with experiment, we constructed the initial microstructure from the measured initial grain size ($R_0 \approx 0.46$ μm), set the pixel step to 0.5 μm, randomly assigned grain orientations, and calibrated the mapping between Monte Carlo steps and real time by repeatedly comparing simulated average grain sizes with the experimental data. As summarized in Fig. 4b, both simulation and experiment follow the classical grain-growth relation $R^n - R_0^n = Kt (n \approx 6.52)$, in good agreement with measurements, confirming that the model reproduces the overall growth trend. It can be observed that grains with lower Young's moduli (e.g., orientation 5) grow faster than those with higher moduli (e.g., orientation 1). Figure 4c shows that, as grains coarsen, the von Mises stress distribution evolves from being concentrated at grain boundaries to a more relaxed state. When accounting for the influence of grain morphology on stress distribution in TGV–Cu, the average von Mises stress in the Cu filling of the TGV decreases with increasing grain size—this is because grain-boundary regions bear higher stress, and smaller average grain sizes entail more boundaries and thus higher overall stress. Notably, high-modulus grains retain higher local stresses than low-modulus grains. Figure 4d shows the system's total free energy decreasing rapidly over the first 200 hours and then leveling off, indicating a gradual approach to thermodynamic equilibrium. Figure 4e shows elastic strain energy decreasing with grain growth. Comparing grain maps (Fig. 4a) and stress fields (Fig. 4c) reveals that "soft" (low-stress) grains preferentially grow, while "hard" (high-stress) grains lag. Overall, the anisotropic mechanical properties of copper grains in the TGV markedly influence thermal-stress distribution during aging: thermal stress drives the preferential growth of grains with low Young's modulus, reducing overall von Mises stress. Consequently, as TGV–Cu ages, the copper within the vias softens, rendering the structure more compliant and susceptible to deformation.

To evaluate the electrical properties of TGV–Cu before and after aging, I-V measurements were performed on cross-sectional samples using a probe station coupled with a Keithley 4200A-SCS parameter analyzer. Twenty-micrometer wafer probes contacted TGV-Cu, applying a voltage sweep from 0 to 10 V. During tests, probes connected to the analyzer through coaxial cables monitored electrical characteristics (Fig. S4). Figure 4f shows linear I–V curves passing through the origin for all aging durations, confirming ohmic conduction without breakdown or threshold-voltage behavior within the tested range. The leakage current of samples at 10 V remained below 10 nA, indicating excellent insulating quality. The unaged sample demonstrated extremely high insulation resistance and negligible leakage current. Insulation resistance decreased rapidly to 2.5 MΩ after 84 hours and further dropped to 1.6 MΩ at 168 hours, then declined more gradually, stabilizing around 500 h and remaining essentially unchanged up to 1008 h. All electrical measurements were carried out in a dry inert ambient, minimizing moisture-enabled ionic conduction. Cross-sectional energy dispersive spectroscopy(EDS) after 1008 h revealed no continuous oxide/reaction layer at the Cu/glass interface (Fig. S5), whereas SEM showed microcracks within the glass adjacent to the interface. These results underscore the excellent electrical performance of the TGV–Cu structure: even after prolonged high-temperature aging, although insulation resistance is reduced, it remains at a high level. Taken together, the stabilized resistance reduction is attributed primarily to stress-assisted microcrack percolation along the Cu/glass

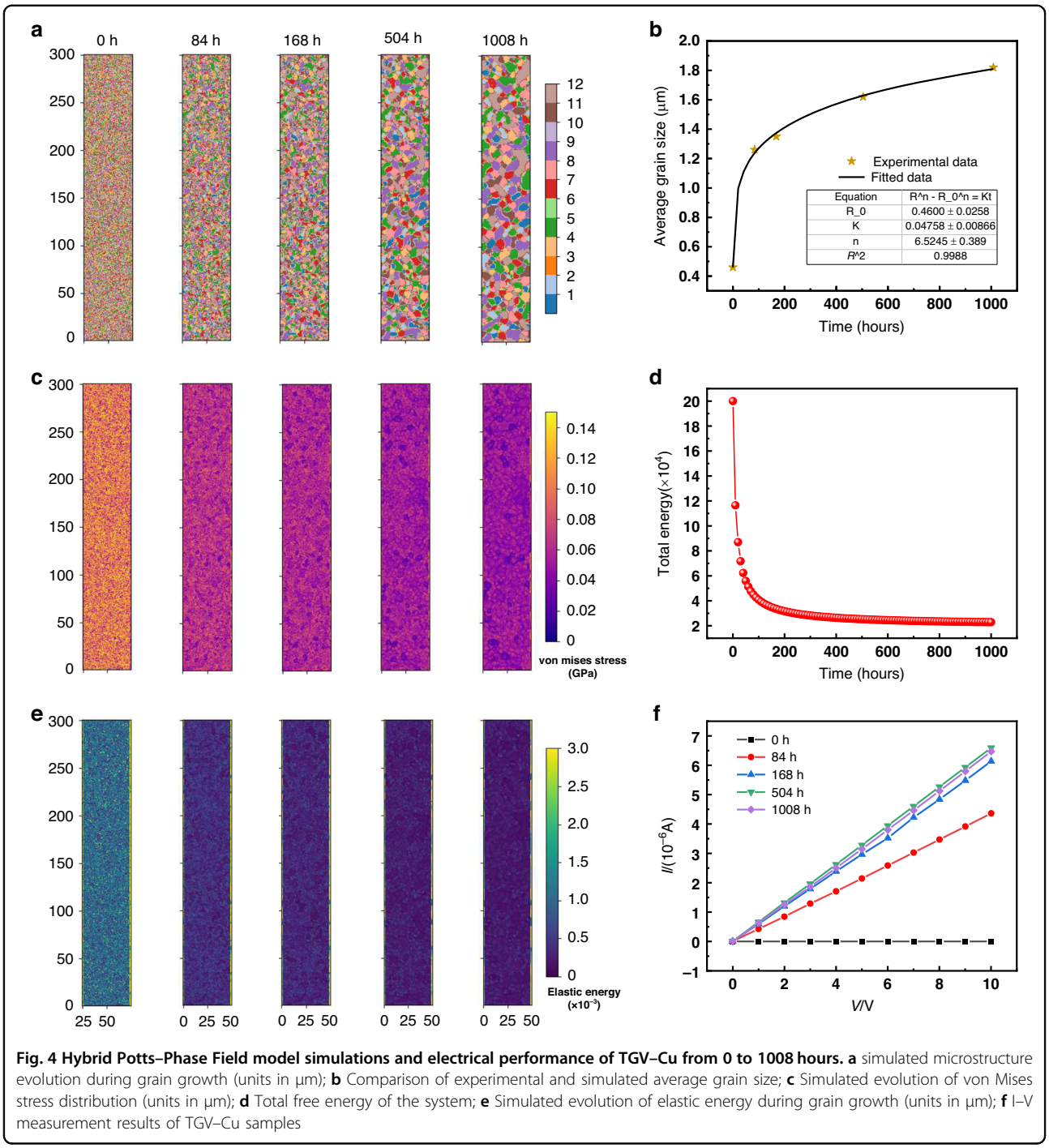


Fig. 4 Hybrid Potts–Phase Field model simulations and electrical performance of TGV–Cu from 0 to 1008 hours. a simulated microstructure evolution during grain growth (units in μm); **b** Comparison of experimental and simulated average grain size; **c** Simulated evolution of von Mises stress distribution (units in μm); **d** Total free energy of the system; **e** Simulated evolution of elastic energy during grain growth (units in μm); **f** I–V measurement results of TGV–Cu samples

vicinity—which locally shortens leakage paths—rather than to a uniform interfacial oxidation or diffusion layer.

Conclusions

Through systematic experimental characterization and computational modeling, this study demonstrates that high-temperature aging at 250 °C profoundly alters the microstructure, mechanical integrity, and electrical performance of electroplated TGV-Cu interconnects. Nanoindentation and EBSD analyses reveal region-dependent softening, with hardness and modulus decreasing most rapidly near via surfaces due to grain coarsening, dislocation annihilation, and stress relaxation. Molecular dynamics simulations theoretically corroborate the inverse relationship between grain size and micro-mechanical strength. We developed a hybrid Q-state Potts-based phase field model that enables

the investigation of the thermo-mechanical behavior of Cu grains with different orientations in TGV during long-term high-temperature aging. The simulation results show that as grains grow, the overall von Mises stress in the structure decreases. However, anisotropic mechanical properties of different grains also significantly affect the stress distribution: low-modulus grains with lower stress levels preferentially grow, causing TGV-Cu to soften and deform more easily during extended aging. Despite minor reductions in insulation resistance after prolonged aging, I–V measurements confirm stable ohmic behavior without breakdown. Collectively, these findings provide a comprehensive framework for predicting the long-term reliability of TGV interposers and offer design guidelines to enhance the robustness of heterogeneous integration platforms.

Methods

Sample preparation

The TGV samples were fabricated on Schott AF32 borosilicate glass substrates using a laser-induced deep etching method. First, a Ti/Cu adhesion/barrier and seed layer was deposited onto the via walls by magnetron sputtering. A copper filling was then performed on both sides by electroplating. After plating, the samples were sequentially cleaned in deionized water and isopropanol via ultrasonic agitation, blown dry with nitrogen, and vacuum-dried at 60 °C. A subsequent anneal at 300 °C for 1 h was applied. Following electrical and mechanical testing, the samples were sectioned to expose a cross-section and reveal the Cu-filled TGV structure. The specimens were ground using SiC papers of grit #80, #120, #400, #600, #800, #1200, and #1500, then mechanically polished with 2.5 μm and 0.5 μm diamond suspensions. Finally, the cross-sections were ion-polished in a Hitachi IM4000 Ion Mill to ensure a smooth, clear surface for microstructural characterization.

Characterization

Nanoindentation tests were performed on a KLA iNano nanomechanical testing system equipped with a diamond Berkovich indenter. To evaluate the effect of 250 °C aging on micromechanical properties, indentations were made at 30 μm intervals across the copper-filled vias. The microstructural evolution of TGV–Cu during aging was analyzed via scanning electron microscopy (SEM) on a Zeiss GeminiSEM 360 at an accelerating voltage of 15 kV. Following indentation, the imprint morphology was characterized using a SENSOFAR 3D optical profiler. To elucidate the influence of high temperature storage on microstructure and its relevance to micro- and nanoscale mechanical behavior, electron backscatter diffraction (EBSD) analyses were conducted on a Thermo Scientific Apreo 2 C field-emission SEM equipped with an EDAX Velocity Super detector at 20 kV, a 6.4 nA probe current, and a step size of 70 nm. Precise localization of the EBSD scan area was achieved by correlating nanoindentation positions with optical microscopy. For each TGV–Cu cross section, EBSD data were collected over the entire via width (10 μm) by length (300 μm). These datasets were analyzed using TSL OIM software to extract grain size, crystallographic orientation, and grain-boundary characteristics.

Simulation

Molecular dynamics (MD) simulations were conducted with the Large-scale Atomic/Molecular Massively Parallel Simulator (LAMMPS). Prior to nanoindentation, the system was equilibrated under isothermal–isobaric (NPT) conditions to achieve zero residual pressure in all spatial directions. The loading and unloading of polycrystalline copper models with varying grain sizes were simulated using an embedded-atom method (EAM) potential to characterize Cu–Cu. Simulation outputs were visualized using OVITO; dislocation types and lengths were quantified via the Dislocation Extraction Algorithm (DXA). The Delft University of Technology ECTM research Group's Q-state Potts phase-field (QPPF) package is used to simulate grain growth. The QPPF package integrates the Taichi (CPU backend) parallel programming language within Python to accelerate large-scale microstructure simulations and capture the long-term dynamics of complex multiphase systems[40].

Acknowledgements

This work was supported by the National Natural Science Foundation of China (Grant No. 52275559) and China Scholarship Council (Grant No. 202406100064).

Author details

[1]Shanghai Engineering Technology Research Center of SiC Power Device, College of Intelligent Robotics and Advanced Manufacturing, Fudan University, Shanghai, China. [2]State Key Laboratory of Precision Electronic Manufacturing Technology and Equipment, Guangdong University of Technology, Guangzhou, China. [3]EEMCS Faculty, Delft University of Technology, Delft, the Netherlands. [4]Guangdong Fozhixin Microelectronics Technology Research Co. Ltd., Foshan, China. [5]Research Institute of Fudan University in Ningbo, Ningbo, China

Author contributions

J.C., X.H., C.C., and J.F. conceived the initial idea and designed the experiments. J.C., B.Y., X.H., Z.Z.L., W.L., X.Y., and C.G. fabricated the samples and carried out the material characterization. J.C., Z.C.L., Z.Y., J.L., G.Y., C.Z., C.C., and G.Z. performed the experimental and theoretical analyses and wrote the manuscript. X.H., C.C., and J.F. edited the manuscript and guided the work. All the authors contributed to discussions.

Conflict of interest

The authors declare no competing interests.

Supplementary information The online version contains supplementary material available at https://doi.org/10.1038/s41378-026-01160-0.

Received: 29 July 2025 Revised: 29 November 2025 Accepted: 22 December 2025
Published online: 02 February 2026

References

1. Shulaker, M. M. et al. Three-dimensional integration of nanotechnologies for computing and data storage on a single chip. *Nature* **547**, 74–78, https://doi.org/10.1038/nature22994 (2017).
2. Das Sharma, D., Pasdast, G., Tiagaraj, S. & Aygün, K. High-performance, power-efficient three-dimensional system-in-package designs with universal chiplet interconnect express. *Nat Electron* **7**, 244–254, https://doi.org/10.1038/s41928-024-01126-y (2024).
3. Liu, F. et al. A Critical Review of Lithography Methodologies and Impacts of Topography on 2.5-D/3-D Interposers. *IEEE Trans Compon. Packag Manuf Technol* **13**, 291–299, https://doi.org/10.1109/TCPMT.2023.3265568 (2023).
4. Chen, J. et al. Review of Inorganic Nonmetallic Materials in Power Electronics Packaging Application. *IEEE Trans Power Electron* **40**, 10509–10530, https://doi.org/10.1109/TPEL.2025.3550882 (2025).
5. Manley, M. et al. Heterogeneous Integration Technologies for Artificial Intelligence Applications. *IEEE J Explor. Solid-State Comput. Devices Circuits* **10**, 89–97, https://doi.org/10.1109/JXCDC.2024.3484958 (2024).
6. Chung, E. et al. Electrical–Thermal Co-Analysis of Through-Silicon Vias (TSVs) Integrated Within Micropin-Fin Heatsink for 3-D Heterogeneous Integration (HI). *IEEE Trans Compon, Packag. Manuf. Technol.* **14**, 1792–1802, https://doi.org/10.1109/TCPMT.2024.3452637 (2024).
7. Sun, Q. et al. Nondestructive monitoring of annealing and chemical–mechanical planarization behavior using ellipsometry and deep learning. *Microsyst. Nanoeng.* **9**, 50, https://doi.org/10.1038/s41378-023-00529-9 (2023).
8. Swaminathan, M. et al. Glass Packaging for 6G Applications. *IEEE Microw. Mag.* **26**, 46–64, https://doi.org/10.1109/MMM.2025.3540325 (2025).
9. Li, X. et al. Glass Package With Multiple Embedded Dies for mmWave Applications. *IEEE Trans. Compon, Packag. Manuf Technol.* **14**, 1816–1824, https://doi.org/10.1109/TCPMT.2024.3453169 (2024).
10. Feng, J. et al. Thermal-electrical coupling effect on the reliability of copper pillar bump joints with different initial IMC thickness and microstructure. *J. Manuf. Process.* **139**, 182–192, https://doi.org/10.1016/j.jmapro.2025.02.026 (2025).
11. Gousseau, S. et al. Electromigration-induced failure in operando characterization of 3D interconnects: microstructure influence. *Microelectron. Reliab.* **55**, 1205–1213, https://doi.org/10.1016/j.microrel.2015.05.019 (2015).
12. Chen, L. et al. Research on high-power high-frequency electrical transmission characteristics of through glass via interconnections. *Microelectron. Reliab.* **172**, 115828, https://doi.org/10.1016/j.microrel.2025.115828 (2025).
13. Hou, M. et al. Wet etching process optimization and consistency enhancement of massive through glass vias through laser-induced wet etching. *IEEE Trans. Compon Packag Manuf Technol* 1-1 https://doi.org/10.1109/TCPMT.2025.3578609 (2025).
14. Wang, M. et al. Effect of heat treatment processes on the Cu-electrodeposited through glass vias (TGV) plate. *J Alloy Compd* **997**, 174928. https://doi.org/10.1016/j.jallcom.2024.174928 (2024).
15. Wang, M. et al. The influence of heat treatment process on electroplated metallized through glass vias (TGV) substrates. *J Alloy Compd* **1035**, 181522. https://doi.org/10.1016/j.jallcom.2025.181522 (2025).
16. Wang, H. et al. Modeling and characterization of annealing effect on the Cu protrusion and thermomechanically behaviors of through glass via. *IEEE Trans Compon Packag Manuf Technol* **14**, 1300–1307, https://doi.org/10.1109/TCPMT.2024.3409908 (2024).
17. Chen, S., An, T., Qin, F. & Chen, P. Microstructure evolution and protrusion of electroplated Cu-filled through-silicon vias subjected to thermal cyclic loading. *J Electron Mater* **46**, 5916–5932, https://doi.org/10.1007/s11664-017-5577-7 (2017).
18. Liang, S. B., Wei, C., Ke, C. B., Zhou, M. B. & Zhang, X. P. in *2017 18th International Conference on Electronic Packaging Technology (ICEPT)*. 1617-1622.
19. Liang, S. B., Ke, C. B., Wei, C., Zhou, M. B. & Zhang, X. P. in *2018 IEEE 68th Electronic Components and Technology Conference (ECTC)*. 2134-2141.
20. Chen, S. et al. Protrusion of electroplated copper filled in through silicon vias during annealing process. *Microelectron Reliab* **63**, 183–193, https://doi.org/10.1016/j.microrel.2016.04.005 (2016).
21. Sonawane, D. & Kumar, P. Role of grain boundary sliding in structural integrity of Cu-filled through Si via during isothermal annealing. *J Electron Mater* **50**, 767–778, https://doi.org/10.1007/s11664-020-08476-1 (2021).
22. Liu, T. et al. Study of the protrusion of through-silicon vias in dual annealing-CMP processes for 3D integration. *Microsyst Nanoeng* **11**, 25, https://doi.org/10.1038/s41378-024-00797-z (2025).
23. Li, Y. et al. Constitutive modelling of annealing behavior in through silicon vias-copper. *Mater Charact* **179**, 111359. https://doi.org/10.1016/j.matchar.2021.111359 (2021).
24. Kadota, H., Kanno, R., Ito, M. & Onuki, J. Texture and grain size investigation in the copper plated through-silicon via for three-dimensional chip stacking using electron backscattering diffraction. *Electrochem Solid-State Lett* **14**, D48, https://doi.org/10.1149/1.3555448 (2011).
25. Yang, Z. et al. Residual stress characterization in microelectronic manufacturing: an analysis based on Raman Spectroscopy. *Laser Photonics Rev* **18**, 2301300. https://doi.org/10.1002/lpor.202301300 (2024).
26. Qian, H., Huang, Z., Zhu, Q., Xu, Y. & Wang, H. Influence of microvoid on fatigue behaviour and crack initiation of TSV-Cu under thermal cyclic loading based on the stored energy density indication. *Eng Fract Mech* **323**, 111205. https://doi.org/10.1016/j.engfracmech.2025.111205 (2025).
27. Li, X., Wei, Y., Lu, L., Lu, K. & Gao, H. Dislocation nucleation governed softening and maximum strength in nano-twinned metals. *Nature* **464**, 877–880, https://doi.org/10.1038/nature08929 (2010).
28. Yang, Z. et al. Prediction of temperature-dependent stress in 4H-SiC using in situ nondestructive Raman Spectroscopy characterization. *Laser Photonics Rev* **19**, 2401033. https://doi.org/10.1002/lpor.202401033 (2025).
29. Xi, Y. et al. The impact of sidewall copper grain condition on thermo-mechanical behaviors of TSVs during the annealing process. *Microsyst Nanoeng* **10**, 194, https://doi.org/10.1038/s41378-024-00830-1 (2024).
30. Liu, H. et al. Review on fatigue of additive manufactured metallic alloys: microstructure, performance, enhancement, and assessment methods. *Adv Mater* **36**, 2306570. https://doi.org/10.1002/adma.202306570 (2024).
31. Shabib, I. & Miller, R. E. Deformation characteristics and stress–strain response of nanotwinned copper via molecular dynamics simulation. *Acta Mater* **57**, 4364–4373, https://doi.org/10.1016/j.actamat.2009.05.028 (2009).
32. Kossman, S., Coorevits, T., lost, A. & Chicot, D. A new approach of the Oliver and Pharr model to fit the unloading curve from instrumented indentation testing. *J Mater Res* **32**, 2230–2240, https://doi.org/10.1557/jmr.2017.120 (2017).
33. Huang, K., Zhang, K., Marthinsen, K. & Logé, R. E. Controlling grain structure and texture in Al-Mn from the competition between precipitation and recrystallization. *Acta Mater* **141**, 360–373, https://doi.org/10.1016/j.actamat.2017.09.032 (2017).
34. Wolf, D., Yamakov, V., Phillpot, S. R., Mukherjee, A. & Gleiter, H. Deformation of nanocrystalline materials by molecular-dynamics simulation: relationship to experiments?. *Acta Mater* **53**, 1–40, https://doi.org/10.1016/j.actamat.2004.08.045 (2005).
35. Tatsumi, H., Kao, C. R. & Nishikawa, H. Atomistic behavior of Cu–Cu solid-state bonding in polycrystalline Cu with high-density boundaries. *Mater Des* **250**, 113576. https://doi.org/10.1016/j.matdes.2024.113576 (2025).
36. Feng, S. et al. Evaluating the electromigration effect on mechanical performance degradation of aluminum interconnection wires: A nanoindentation test with molecular dynamics simulation study. *Appl Surf Sci* **676**, 160992. https://doi.org/10.1016/j.apsusc.2024.160992 (2024).
37. Jiang, T. et al. Plasticity mechanism for copper extrusion in through-silicon vias for three-dimensional interconnects. *Appl Phys Lett* **103**, 211906. https://doi.org/10.1063/1.4833020 (2013).
38. Hu, X. et al. in *2025 IEEE 75th Electronic Components and Technology Conference (ECTC)*. 699-704.
39. Homer, E. R., Tikare, V. & Holm, E. A. Hybrid Potts-phase field model for coupled microstructural–compositional evolution. *Comput Mater Sci* **69**, 414–423, https://doi.org/10.1016/j.commatsci.2012.11.056 (2013).
40. Hu, Y., Li, T. M., Anderson, L., Ragan-Kelley, J. & Durand, F. Taichi: a language for high-performance computation on spatially sparse datastructures. *ACM Transactions on Graphics (TOG)* **38**, 1–16, https://doi.org/10.1145/3355089.3356506 (2019).